Differences of characteristics and performance with Bi3+ and Bi2O3 doping over TiO2 for photocatalytic oxidation under visible light

Article

Accepted Version

Differences of characteristics and performance with Bi^{3+} and Bi_2O_3 doping over TiO_2 for photocatalytic oxidation under visible light

Qiong Huang[1, *], Juan Ye[1], Han Si[1], Bo Yang[1], Tao Tao[1], Yunxia Zhao[1], Mindong Chen[1] and Hong Yang[1, 2, *]

[1] Jiangsu Collaborative Innovation Center of Atmospheric Environment and Equipment Technologies, Jiangsu Key Laboratory of Atmospheric Environmental Monitoring & Pollution Control, School of Environmental Science & Engineering, Nanjing University of Information Science & Technology, Nanjing 210044, China;

[2] Department of Geography and Environmental Science, University of Reading, Whiteknights, Reading, RG6 6AB, UK

*Corresponding author 1: Dr. Qiong Huang

School of Environmental Science and Engineering, Nanjing University of Information Science & Technology, Nanjing 210044, China

Address: No. 219 Ningliu Road, Nanjing University of Information Science & Technology, School of Environmental Science and Engineering, 210044, Nanjing, China

E–mail: hqhaixia@163.com (Q.H.)

Tel: +86 25 58731090 Fax: +86 25 58731090

*Corresponding author 2: Dr. Hong Yang

Department of Geography and Environmental Science, University of Reading, Whiteknights, Reading, RG6 6AB, UK

E–mail: hongyanghy@gmail.com (H. Y.)

Tel: +44 (0)1183787750

Differences of characteristics and performance with Bi^{3+} and Bi_2O_3 doping over TiO_2 for photocatalytic oxidation under visible light

Abstracts: Bi-doped TiO_2 photocatalysts were synthesized by sol with a high-pressure hydrothermal method and developed for the photocatalytic degradation of formaldehyde under the visible light irradiation and ambient temperature. According to characterization, it could be found that some Bi-doped TiO_2 could be transformed into the distinctive crystals phase of $Bi_4Ti_3O_{12}$, which was crucial for improving activity. The excess Bi_2O_3 doping into TiO_2, such as Bi_2O_3-N/TiO_2 and Bi_2O_3-C/TiO_2, generated a mixed oxides with Bi_2O_3 and $Bi_4Ti_3O_{12}$, was not beneficial to increase the activity of HCHO oxidation, whereas Bi^{3+}/TiO_2 composed of TiO_2 and $Bi_4Ti_3O_{12}$ displayed a higher activity with good stability. It was worth noteworthy that Bi^{3+}/TiO_2 didn't show the lowest binding energy. However, it exhibited a lower PL intensity, higher adsorption, and activity due to the uniform particulates, high surface areas, and the strong interaction between TiO_2 and $Bi_4Ti_3O_{12}$, attributing to create superoxide radical anion ($^{\bullet}O_2^-$) and hydroxyl radical (•OH). The present results of Bi^{3+}/TiO_2 indicated that HCHO could be effectively oxidized from 1.094 to 0.058 mg/m^3 (94.7%) under visible light irradiation within 36 h. The current research made effort to draw out the existing state of Bi, which would be better, Bi^{3+} or Bi_2O_3, doped in the TiO_2.

Keywords: TiO_2; Bi-doped; Photocatalytic oxidation; Formaldehyde; Visible light

1. Introduction

With the rapid development of economy and urbanization, decoration has turn into a kind of popular lifestyle. A large number of new decorative materials and furniture have been used in rooms, while they can release a variety of volatile organic compounds (VOCs), such as formaldehyde [1, 2], benzene [3, 4], toluene [5, 6] and so on [7]. Accordingly, indoor air pollution has become an increasingly serious problem. As people spend more time indoors than outdoors, people may suffer from a serious of greater impact on human health, including nausea, dizzy, headache, leukemia, and even cancer [8]. In particular, formaldehyde (HCHO), one of the notorious carcinogenic and deformity-causing substances identified by the World Health Organization (WHO), has been detected at elevated levels in various indoor environments [9]. Hence, seeking an effective method to remove indoor HCHO has been an urgent task. To date, the main strategies of eliminating HCHO include adsorption [10], photocatalysis [11, 12], low temperature plasma [13], and catalytic oxidation at ambient temperature [14]. Considering efficiency and practicality, photocatalytic oxidation using TiO_2 semiconductors is one of advanced technologies and it is still receiving attentions from many researches [15, 16]. Up to now, TiO_2 is still the most frequently used photocatalyst due to the high solar sensitivity, chemical stability and low toxicity [17]. In addition, its high density of states in bands enables the efficient photo to current conversion, and this makes TiO_2 more active than other semiconductors, such as ZnO, SnO_2, ZrO_2, CdS and g-C_3N_4 [18]. Therefore, TiO_2 has been widely applied in various photocatalytic fields, such as water and gas stream treatment, and organic contaminant decomposition [19, 20]. However, owing to its large band gap energy of 3.2 eV (λ<380nm), TiO_2 absorbs only ultraviolet light rather than more visible light that including a large part of solar irradiation [21, 22]. Furthermore, the overall quantum yield rate can be seriously impacted by the low electron transfer rate and a high recombination rate of photo-induced electrons and holes. In order to overcome those problems, lots of efforts have been made to adjust the properties of TiO_2 with electronic, for example, the noble metal deposition [22], the other semiconductor coupling [23], and metal cations or non-metal anions doping [24-27]. Coupling of TiO_2 with Bi_2O_3 [28], as a promising semiconductor, has been found to be a

good strategy for elongating the light region to the visible and enhancing the photocatalytic activity [29]. Bi_2O_3 is an excellent material for the photocatalytic oxidation due to its narrow band gap of 2.8 eV and diversity in crystal structure with doping of TiO_2. Some studies about the Bi_2O_3/TiO_2 composite or Bi-doped TiO_2 found better performance of VOCs photocatalytic oxidation under the excitation of visible light [30]. However, it is still unclear about the existence state of bismuth to improve the oxidation activity over Bi-doped TiO_2, especially for Bi^{3+} or Bi_2O_3, which donate as composite oxides (Bi_xTiO_y), or mixed oxides (Bi_2O_3-TiO_2), separately. Murcia-Lopez et al. [31] synthesized a series of Bi^{3+}-doped TiO_2 catalysts with 2wt% doping to evaluate the photocatalytic oxidation of phenol under UV–vis illumination and they found that the nominal content of Bi^{3+} in TiO_2 was the main reason for the increase in the photocatalytic activity. Bentouami et al. [32] also found that the binding energy of Bi detected by XPS wasn't the same as the one of Bi in Bi_2O_3, and the shift in binding energies of XPS could be ascribed to some valence states higher than Bi^{3+}. Bouattour et al. [33] and Xu et al. [34] suggested that the doped Bi ions substitute some of the titanium atoms in the form of compound oxidation, such as Ti-O-Bi, $Sr_{1-x}Bi_xTi_{1-x}Fe_xO_3$, and $BiFeO_3$, according to the results of XRD and XPS. Kang et al [35] found that Bi ions inserted into TiO_2 could markedly improve CO_2 reduction to CH_4 due to the inhibited recombination of photogenerated electron-hole. However, some scholars had a different opinion that Bi_2O_3 rather than Bi^{3+} played an important role in the photocatalytic oxidation over Bi-doped TiO_2. For instance, Li et al. [36] found that the flower-like Bi_2O_3/TiO_2 with enrichment Bi_2O_3 quantum dots on the surface of photocatalyst exhibited higher activity due to the strong interaction between Bi_2O_3 and TiO_2. Leung [37] and Wang [38] et al. hold that heterojunction structures with mixed semiconductors, such as $TiO_2/ZnO/Bi_2O_3$, 3D $BiOCl_xBr_{1-x}$/graphene oxide, could effectively improve the separation efficiency of photogenerated electron/hole and increase the subsequent photocatalytic activity. Meanwhile, some researcher suggested that bismuth might coexist in the form of Bi^{3+} and Bi_2O_3 over Bi-doped TiO_2 photocatalysts. Li et al. [39] reported an ordinary approach, doping Bi_2O_3 powder into TiO_2 sol, to synthesis Bi-doped TiO_2 photocatalyst. When the loading of Bi_2O_3 exceed 5mol%, $Bi_2Ti_4O_{11}$ phase

started to appear and showed a good crystallization. The calcination temperature had a key effect on the chemical state of Bi, a direct effect on the photocatalytic activity. Attributed to the synergetic effect of Bi_xTiO_y and TiO_2, the photocatalytic activity over Bi-doped TiO_2 could be improved. Gao et al. [30] found that $Bi_4Ti_3O_{12}$ and Fe-doped $Bi_4Ti_3O_{12}$ nanosheets, described with a formula of $(Bi_2O_2)^{2+}(Bi_2Ti_3O_{10})^{2-}$, which was constructed with a TiO_6 octahedral and a $(Bi_2O_2)^{2+}$ monolayer, displayed a high photocatalytic oxidation of bisphenol A and phenol, although not as good as Au-2%Fe/ $Bi_4Ti_3O_{12}$ composite photocatalysts. According to the XPS analysis, XPS signals of Bi_2O_3 powders could also be found. Prabhakaran et al. [40] reported that Bi-doped and Bi–N co-doped TiO_2 nanocomposites could exhibit preferable photocatalytic activities for fabric dye under visible light illumination. However, the results of XRD were different from the results of XPS. XRD spectra showed crystalline Bi_2O_3, while the positive shift of XPS peaks corresponding to $Bi4f_{7/2}$ and $Bi4f_{5/2}$ might also be ascribed to Bi-O-Ti bonds formation on the photocatalyst surface.

To summarize, it is still difficult to clarify the state of Bi, as composite oxides or mixed oxides, for obtaining a high activity over Bi-doped TiO_2 photocatalysts. I t is still necessary to investigate the state of Bi in-depth and find the rules between bismuth and TiO_2 in Bi-doped TiO_2 with composite oxides or mixed oxides. The most attractive aspect of these photocatalysts is the synergistic combination of bismuth oxide and titanium oxide, as doped Bi ions substitute titanium atoms in the form of compound oxidation or doped Bi_2O_3 with TiO_2 in the form of heterojunction structure. Different from previous studies that some simple approaches have been developed to synthesize Bi-doped TiO_2 photocatalysts with the formation of Bi_xTiO_y or Bi_2O_3-TiO_2, bismuth and titanium oxide with composite oxides or mixed oxides were produced for photocatalytic oxidation of low concentration of HCHO under visible light irradiation in this study. The possible mechanism of photocatalytic activities of Bi_xTiO_y and Bi_2O_3-TiO_2 was discussed. This research provides a better understanding of the different composite oxides or mixed oxides in the process of photocatalytic oxidation of HCHO.

2. Materials and Methods

2.1. Syntheses of photocatalysts

All reagents, such as ethanol, glycerol and acetic acid, were analytical grade and were used without further purification in the experiments. For comparison, three different types of Bi-doped TiO_2 photocatalysts were prepared.

The first one was for Bi^{3+}/TiO_2 as composite oxides. 14.3 mL tetrabutyl titanate was added into 8.5 mL ethanol and 8.5 mL glycerol in a conical flask, denoted as solution A with a constant magnetic stirring. 3.2 g bismuth nitrate ($Bi(NO_3)_3 \cdot 5H_2O$) and 0.4 g ammonium carbonate ($(NH_4)_2CO_3$) were dissolved into 8.5 mL ethanol, 8.5 mL glycerol and 6.6 mL acetic acid, denoted as solution B with the magnetic mixture. Later, the solution B dropped into solution A with constant agitation. The resulting solution was stirred for 30 min and transfer into a stainless steel reactor for 2 days aging at 110 ^oC. Finally, the precipitate was centrifuged and scrubbed with using distilled water and ethanol for three times, and then dried at 80 ^oC for 2.5 h and calcined at 450 ^oC for 8.5h [41].

The second were for Bi_2O_3-C/TiO_2 and Bi_2O_3-N/TiO_2 as composite/mixed oxides. 3.2 g bismuth nitrate ($Bi(NO_3)_3 \cdot 5H_2O$) was added into 100 mL distilled water with magnetic stirred until complete dissolution. 30 mL of 4M NaOH aqueous solution was dropped until the pH at 12. With a continuous stirring for 12 h, the suspension was centrifuged and washed with distilled water twice, and then dried at 60 ^oC and calcined at 450 ^oC for 4h, denoted as Bi_2O_3-C powders, or not calcined at 450 ^oC for 4h, denoted as Bi_2O_3-N powders, to obtain two different powders (Bi_2O_3-C and Bi_2O_3-N). After that, another solution was prepared with the same way as Bi^{3+}/TiO_2 without bismuth nitrate, and then these Bi_2O_3-C or Bi_2O_3-N powders were added into the mixed solution together under constant agitation. After that, the resulting solution was stirred for 30 min and transfer into a stainless steel reactor for 2 days aging at 110 ^oC. Finally, the precipitate was centrifuged and scrubbed with using distilled water and ethanol for three times, and then dried at 80 ^oC for 2.5 h and calcined at 450 ^oC for 8.5h. These catalysts were identified as Bi_2O_3-C/TiO_2 and Bi_2O_3-N/TiO_2.

The third one was for Bi_2O_3-TiO_2 as mixed oxides. Two types of powders, such as Bi_2O_3-N and TiO_2, were synthesized in the same way as above. And then, these two kinds of Bi_2O_3-N and TiO_2 powders were mixed with mechanical blending, confirmed

as Bi_2O_3-TiO_2.

2.2. Characterization

The crystal structures of three different styles of photocatalysts were all detected by using a D/max-RB X-ray diffractometer (XRD, D8 Advance, Bruker, Germany) equipped with Cu Kα radiation (λ = 0.15406 nm) in a 2θ range of 10-80° and the scanning speed was 4°/min. Raman spectra were measurement on Renishaw inVia Raman systems at ambient temperature and fitted with the 532 nm line of an Ar ion laser as an excitation source. The microscopic morphological structure and particle size of these prepared samples were observed by using a scanning electron microscope (SEM, Hitachi S-4800, Hitachi, Japan) and a transmission electron microscope (TEM, JEM-2100, JEOL, Japan). The Brunauer-Emmett-Teller (BET, ASAP-2020, Micromeritics Instrument Corporation, USA) surface areas of the spent catalysts and pre-treated were determined by using nitrogen adsorption at 77.3 K. The UV-vis spectra (UV-vis, Lambda 950, Perkin-Elmer, USA) of samples were recorded with an integrating sphere attachment. The scanning range was between 250 nm and 800 nm, and $BaSO_4$ was used as a reference. The excited states of these catalysts composite were detected with photoluminescence (PL, MicOS, HORIBA Scientific, USA). In-situ diffuse reflectance infrared transform spectrometry (DRIFTS, Nicolet 6700FTIR, Thermo, USA) was carried out on a spectrometer fitted with a MCT detector and a high-temperature reaction chamber, which could supply all the necessary gas inlets or outlets and allow for measuring and controlling the temperature. The spectra could be acquired with an accumulation of 64 scans and a resolution of 4 cm^{-1}. IR spectra (Nicolet 410 FTIR, Thermo, USA) on KBr pellets of the samples were recorded on a spectrometer at a resolution of 4 cm^{-1}. The concentration of the samples in KBr was maintained at approximately 0.3%. The X-ray photoelectron spectroscopy (XPS, AXIS ULTRA DLD, Shimadzu-Krotos, Japan) spectra were obtained by using an AlKα X-ray source (1486.6 eV) operated at 15 kV and 300 W with an ESCALAB250 Thermo VG to understand the chemical binding energies of the Bi, Ti and O. Electron paramagnetic resonance (EPR, JES-FA200, JEOL, Japan) spectra was collected from a spectrometer with employing an X-band microwave frequency (9.43GHz) and power (1.5mW) at room

temperature.

2.3. Activity evaluation of HCHO removal

The photocatalytic degradation of HCHO over Bi-doped TiO_2 catalysts was carried out in a self-designed glass reactor (600×600×600 mm). 1mL HCHO (38wt%) was dropped into a petri dish and removed into this glass reactor for five minutes. When the concentration was 1.05 ± 0.05 mg/m^3, the petri dish was moved out and another petri dish with 0.4g photocatalyst powder was transferred into the glass reactor quickly. After that, the glass reactor was immediately sealed by using a glass cover with vaseline. Through a small hole in the front of the glass reactor, the concentration of formaldehyde was detected by using a formaldehyde meter (PPM-400st, PPM Technology, UK), which designed to measure HCHO concentrations from 0 to 24.56 mg/m^3 in snatch samples of air. A 36W energy-saving lamp (LED) providing the visible light was fixed 10cm above the catalyst. When the concentration became stable and the adsorption-desorption equilibrium remained, the energy-saving lamp was turned on and HCHO concentration was measured using the PPM-400st meter for three times at every 12 h. To investigate the photocatalytic activity of different catalysts, a set of gaseous experiments were carried out in the indoor environment.

3. Results and discussion

3.1 The activity of Bi-doped TiO_2 for HCHO oxidation

Fig. 1 shows the conversion of HCHO and stability under visible light irradiation over different types of Bi-doped TiO_2 photocatalysts as a function of time. The conditions in standard tests were composed of HCHO concentration (1.05 ± 0.05 mg/m^3), reaction temperature (20-30ºC), LED type (36 W) and catalyst powder (0.40 g). In terms of the blank and adsorption tests over TiO_2, Bi_2O_3 and Bi^{3+}/TiO_2 catalysts under dark, the concentration of HCHO decreased from 1.052 to 0.923 mg/m^3 at 48h in the blank (Fig. 1 (A)), indicating that the glass reactor owned good airtightness without HCHO leakage. Although the Bi^{3+}/TiO_2 photocatalysts exhibited better adsorption than TiO_2 and Bi_2O_3, the adsorption amount of HCHO was still very low, even negligible. In terms of the photocatalytic activity and stability over these Bi-doped TiO_2 catalysts, the photocatalytic activity and stability of Bi^{3+}/TiO_2 were significantly higher than other

three kinds of Bi-doped TiO_2 catalysts due to the composition and structure (Fig. 1(B) and (C)). The HCHO concentration decreased from 1.094 to 0.058 mg/m^3 at 36h, even below the limits value of standard (0.08 mg/m^3). Moreover, the catalyst demonstrated good stability with four consecutive tests. However, Bi_2O_3-N/TiO_2, Bi_2O_3-C/TiO_2, and Bi_2O_3-TiO_2 catalysts showed the same activity for HCHO degradation and the conversion was about 50% at 48h. Meanwhile, the stability of Bi_2O_3-N/TiO_2 was as bad as its oxidation activity, without improving. Owing to the rapid recombination of photogenerated electrons and holes, although Bi_2O_3 owned lower band gap energy (2.9 eV) than TiO_2 (3.2 eV), it exhibited the lowest activity for HCHO oxidation.

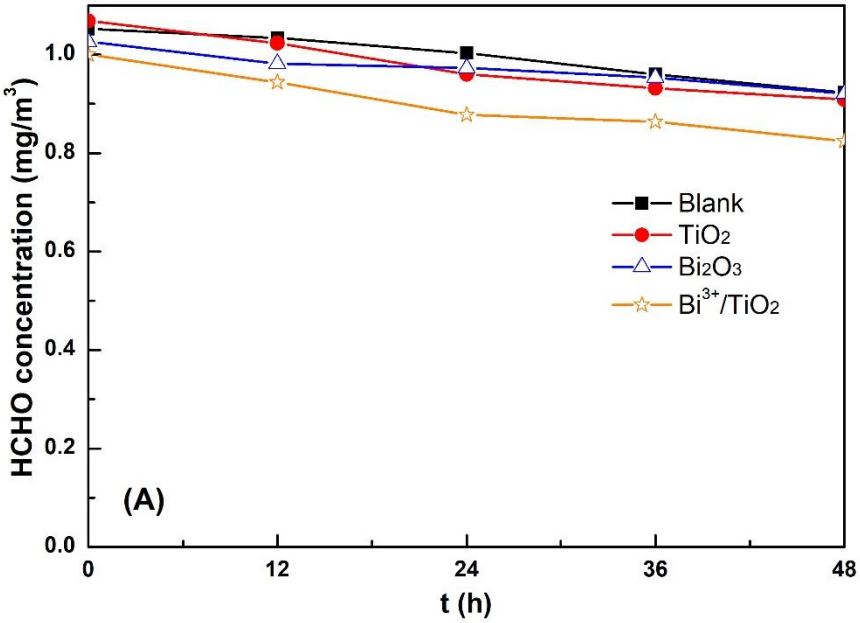

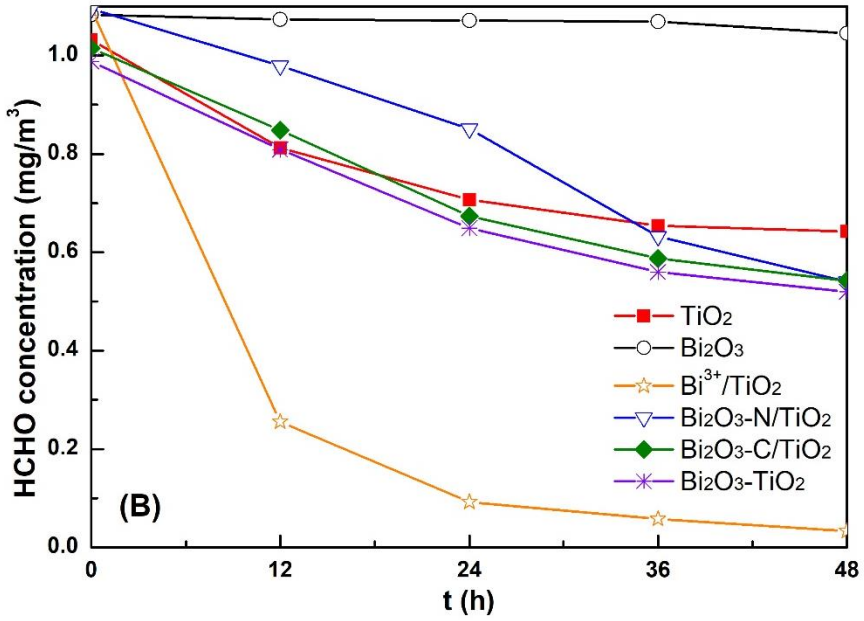

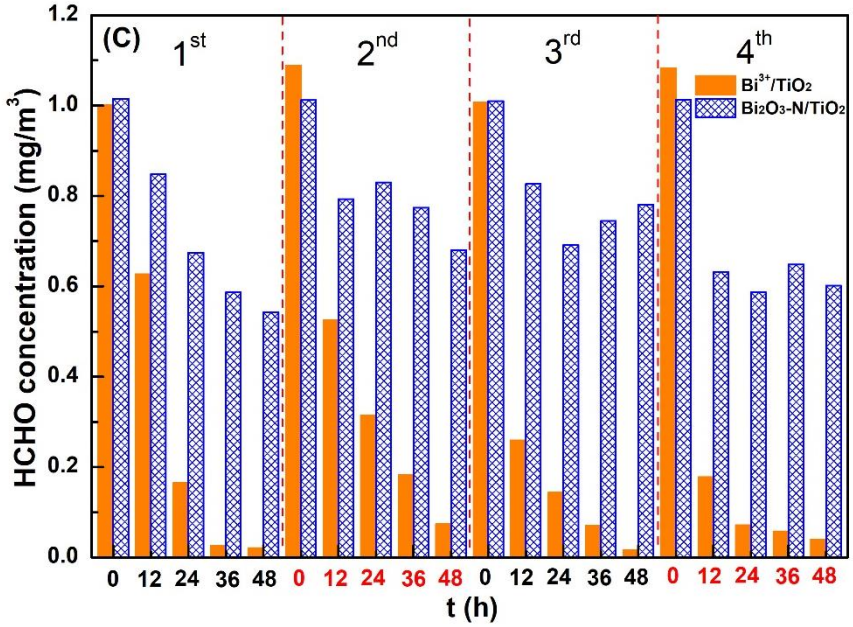

Fig. 1. Photocatalytic degradation of HCHO and stability over Bi-doped TiO_2 catalysts (A: blank and adsorption experiments under dark; B: photocatalytic oxidation of HCHO over Bi-doped TiO_2 catalysts; C: stability experiments over Bi^{3+}/TiO_2 and Bi_2O_3-N/TiO_2 with four times)

3.2 XRD analysis

Fig. 2 shows the XRD patterns of Bi-doped TiO_2 catalysts with different preparation methods calcinated at 450 ºC for 8.5 h. For comparison, the XRD patterns of the as-prepared pure Bi_2O_3 and TiO_2 were also provided. The XRD patterns of TiO_2 and Bi_2O_3 were corresponded to the anatase phase of TiO_2 (PDF # 21-1272) and the monoclinic phase of α-Bi_2O_3 (PDF # 41-1449), respectively. Both of them showed good crystal

structures with the sharp diffraction peaks accompanied by calcinating at 450 °C for 8.5 h and the crystal peaks were calculated by using the Scherrer equation attributed to (1 0 1) and (1 2 0) planes to be 11.9 nm and 84.3 nm. In terms of Bi-doped TiO_2 catalysts, except for Bi_2O_3-TiO_2 mixed oxides, the XRD patterns of Bi^{3+}/TiO_2 were assigned to anatase TiO_2 and a new characteristic peak at 30.2° and 33.1° ascribed to the composite oxide of $Bi_4Ti_3O_{12}$ (PDF # 35-0795). Regarding Bi_2O_3-N/TiO_2 and Bi_2O_3-C/TiO_2 catalysts, the XRD patterns displayed almost the same diffraction peaks indexed to the monoclinic phase of α-Bi_2O_3 and the composite oxide of $Bi_4Ti_3O_{12}$, implying that Bi_2O_3 with calcining or not had no effect on the crystal structure. This is due to that these two kinds of Bi-doped TiO_2 catalysts composed of Bi_2O_3 and $Bi_4Ti_3O_{12}$ led to a lower activity than Bi^{3+}/TiO_2. In terms of Bi_2O_3-TiO_2 mixed oxide catalyst, the diffraction peaks in the patterns were ascribed to the TiO_2 and α-Bi_2O_3, respectively. Therefore, the above results indicated that the heterojunction structure with TiO_2 and $Bi_4Ti_3O_{12}$ was the critical factor to obtain a high activity for HCHO oxidation, rather than the incorporation of Bi_2O_3 and $Bi_4Ti_3O_{12}$, even with Bi_2O_3 and TiO_2.

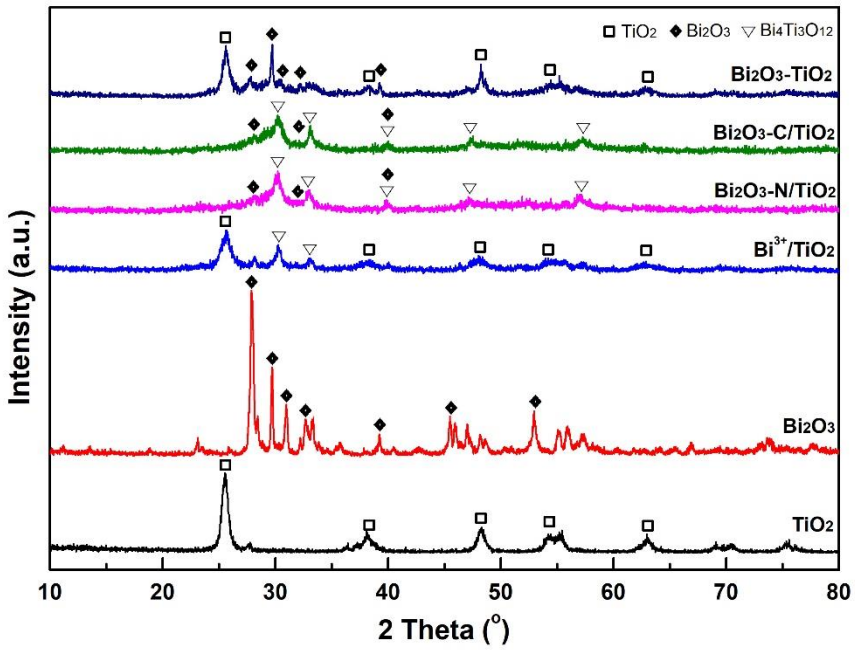

Fig. 2. XRD patterns of TiO_2, Bi_2O_3, and Bi-doped TiO_2 catalysts

3.3 BET analysis

Table 1. Textural properties of TiO_2, Bi_2O_3, and Bi-doped TiO_2 catalysts

Samples	S_{BET} (m^2/g)	V_p (cm^3/g)	d_p (nm)
TiO_2	59.53	0.11	5.76
Bi_2O_3	37.96	0.03	5.43
Bi^{3+}/TiO_2	52.39	0.12	7.82
Bi_2O_3-N/TiO_2	27.3	0.07	6.73
Bi_2O_3-C/TiO_2	42.78	0.10	7.23
Bi_2O_3-TiO_2	50.51	0.11	6.67

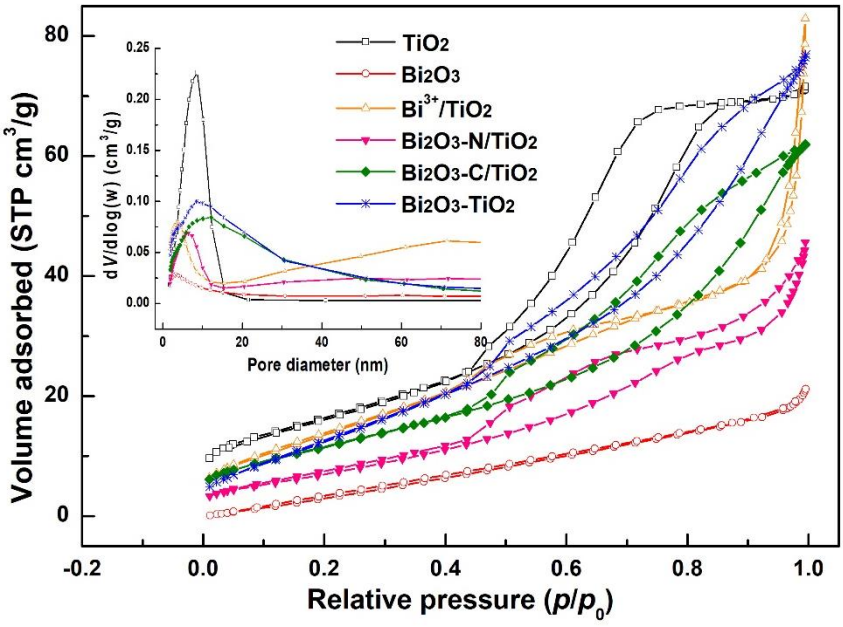

Fig. 3. Nitrogen adsorption-desorption isotherms and pore-size distribution curves of TiO_2, Bi_2O_3, and Bi-doped TiO_2 catalysts

In general, the large surface areas of catalysts can provide more active sites to adsorbent reactant molecules and then oxidize, which can effectively improve the activity of HCHO oxidation. Fig. 3 shows N_2 adsorption-desorption isotherms and the appropriate pore size distribution curves of different types of Bi-doped TiO_2 catalysts. The isotherms of TiO_2 displayed a type IV isotherm with a H2 hysteresis loops, which may include typical "ink bottle" holes, tubular holes with uneven pore size distribution, or densely packed spherical particle interstitial holes, etc. Bi-doped TiO_2 catalysts, except for Bi^{3+}/TiO_2, showed adsorption-desorption isotherms of type IV with an overlap of H2 and H3 hysteresis loops, resulting from bottle-ink and slit-like pores, signifying that the pore sizes of these samples lied in the range of 2–50 nm. The result could also be

confirmed by the pore size distribution and the result of BET (Table 1) and SEM (Fig. 5), which demonstrated that the pore sizes of these samples were from 5 to 8 nm. However, Bi^{3+}/TiO_2 displayed two distinct hysteresis loops, implying that one of the hysteresis loops was the channel in these particles and the other should be the accumulation hole of the particles. The result implied that Bi^{3+}/TiO_2 had larger channels, which was also confirmed by the pore size distribution and the improved HCHO adsorption. Bi^{3+}/TiO_2 (S_{BET}=52.39 m^2/g) exhibited the largest surface areas and pore sizes among these different types of Bi-doped TiO_2 catalysts. In addition, the surface areas of TiO_2 and Bi_2O_3 were calculated to be 59.53 m^2/g and 37.96 m^2/g, respectively. Bi_2O_3 and Bi_2O_3-N/TiO_2 exhibited extremely low pore volume, which were aligned with the adsorption-desorption isotherms, and these could significantly decrease the adsorption of HCHO and be detrimental for the improvement of oxidation activity. Therefore, the above results demonstrated that the specific surface areas maybe not the most important factor for photocatalytic oxidation of HCHO, but it could display a minor role in the activity enhancement.

3.4 Raman analysis

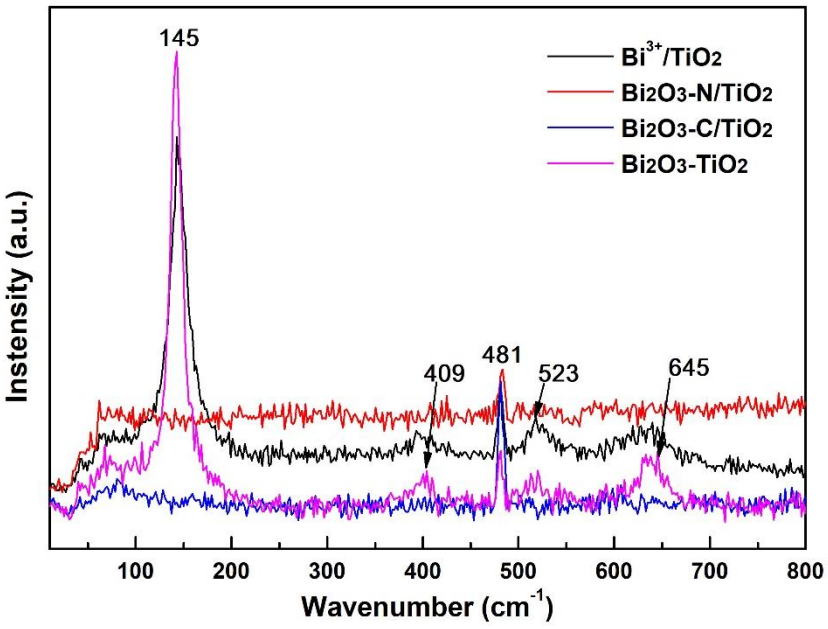

Fig. 4. Raman spectra of Bi-doped TiO_2 catalysts

Fig. 4 shows the Raman spectra of Bi-doped catalysts with different synthetic methods. The peaks at 145, 409, 523 and 645 cm^{-1} could be identified to the characteristic bands

of anatase TiO_2 [39], indicating that the TiO_2 was one of the main phase structures in the sample of Bi^{3+}/TiO_2 and Bi_2O_3-TiO_2, which was consistent with the XRD results. While for Bi_2O_3-N/TiO_2 and Bi_2O_3-C/TiO_2, it was difficult to detect the presence of anatase TiO_2 by Raman spectra. More importantly, the Raman peak at 481 cm^{-1} could be assigned to the characteristic band of Bi_2O_3. Among these samples, the Bi_2O_3-C/TiO_2 exhibited the strongest intensity due to Bi_2O_3 powder calcined at 450 ^oC for 4h. While for Bi_2O_3-N/TiO_2, Bi_2O_3-C/TiO_2 and Bi^{3+}/TiO_2, it was easy to find the presence of $Bi_4Ti_3O_{12}$, not Bi_2O_3, by the XRD measurement, which was not corroborate well with Raman spectra. That was because the composite oxides of $Bi_4Ti_3O_{12}$ contained the characteristic band of Bi_2O_3.

3.5 Morphology measurement

The morphology structure of TiO_2, Bi_2O_3, and Bi-doped TiO_2 catalysts were investigated by using SEM and TEM. TiO_2 showed an aggregated of lumpy particles with a smooth surface, while Bi_2O_3 displayed some aggregated and smaller particles with a rough surface attributed to nano-sized spherical Bi_2O_3 (Fig. 5(B)). Bi_2O_3-TiO_2 (Fig. 5(C)) mixed oxides with TiO_2 and Bi_2O_3 exhibited the same image as the images of Fig. 5(A) and Fig. 5(B) without changing. Regarding Bi-doped TiO_2 catalysts (Fig. 5(D-F)), SEM image of Bi^{3+}/TiO_2 composites that were composed of mutually aggregated spherical nanoparticles showed a uniform particulate state and it could improve the adsorption of visible light and HCHO to increase the activity. While, samples of Bi_2O_3-N/TiO_2 and Bi_2O_3-C/TiO_2 calcined at 450 ^oC for 8.5h displayed irregular and smooth-surfaced lumps, indicated that there was a melting-recrystallization-remelting process for these composites. As can be seen in Fig. 5(G), the observed lattice spacing of 0.234 nm was attributed to the (0 14 0) crystal planes of $Bi_4Ti_3O_4$, and lattice spacing of 0.243 nm and 0.166 nm (not shown) corresponded to the (1 0 3) and (2 1 1) crystal planes of anatase TiO_2, respectively. However, the images of Bi_2O_3-N/TiO_2 and Bi_2O_3-C/TiO_2 catalysts exhibited that these particles aggregated together and produced a large number of lumps with a smooth surface due to roasted Bi_2O_3 without doping into TiO_2. According to Fig. 5(H), the lattice spacing of 0.234 nm, 0.271 nm, 0.269 nm and 0.256 nm matched well with the (0 14 0) crystal planes of

$Bi_4Ti_3O_4$ and the (-1 2 2), (2 2 0), and (-2 1 2) crystal planes of Bi_2O_3 (not shown). The above results were all in accordance with the XRD exhibited in Fig. 2.

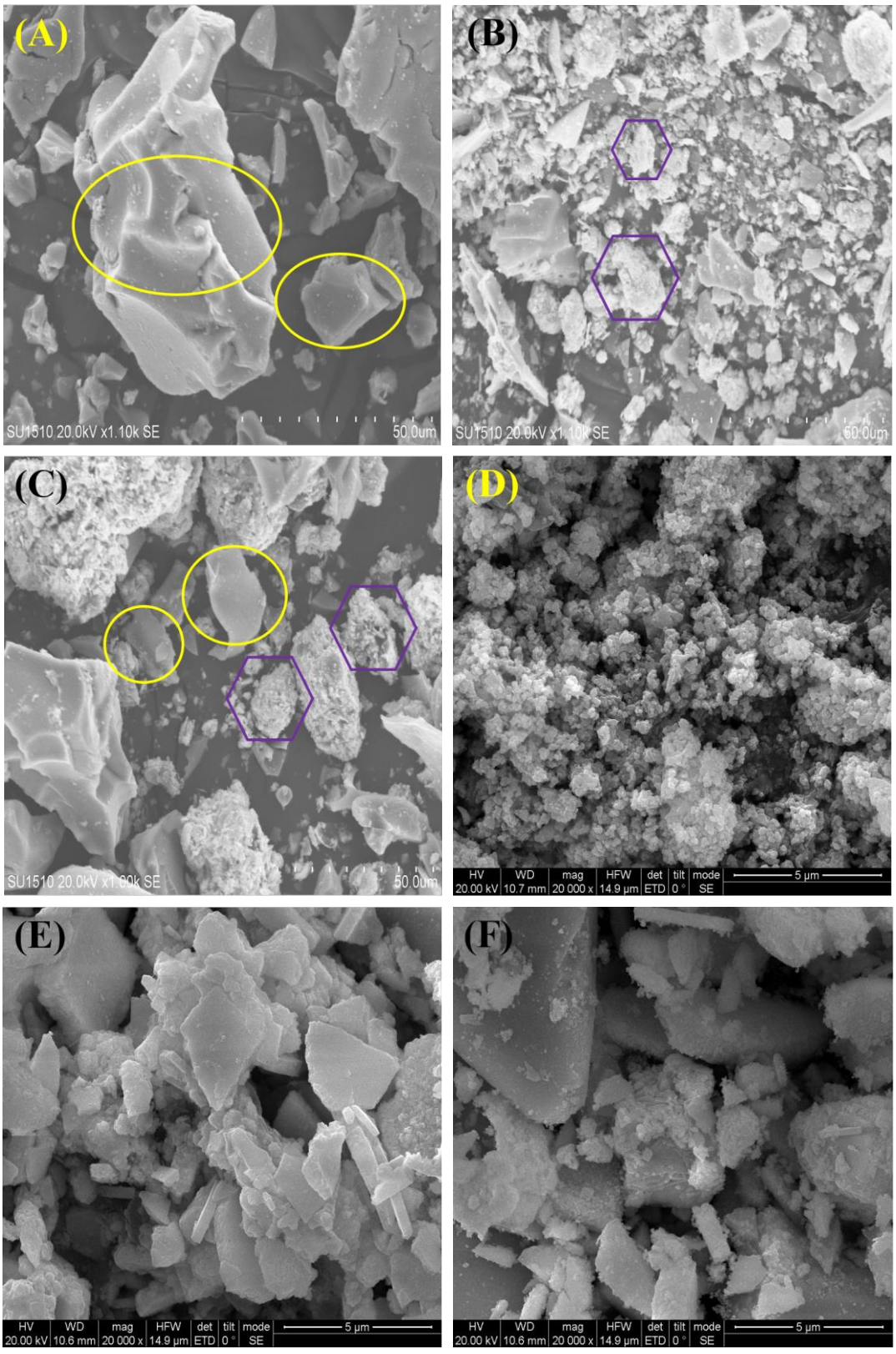

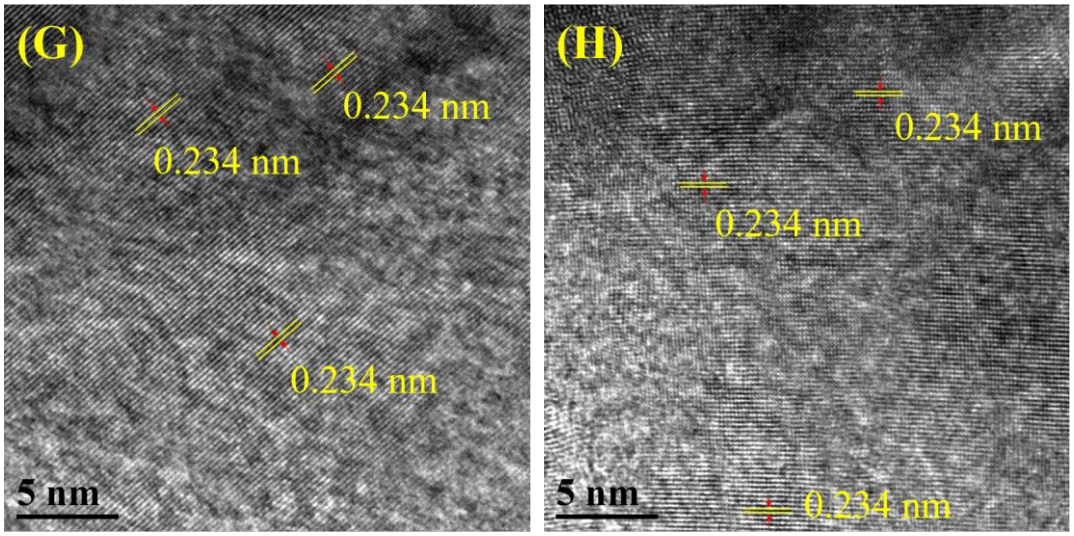

Fig. 5 SEM and TEM images of photocatalysts: (A) TiO_2, (B) Bi_2O_3, (C) Bi_2O_3-TiO_2, (D, G) Bi^{3+}/TiO_2, (E, H) Bi_2O_3-N/TiO_2, and (F) Bi_2O_3-C/TiO_2

3.6 Optical absorption properties

The corresponding UV-vis DRS and PL spectra of TiO_2, Bi_2O_3 and Bi-doped TiO_2 catalysts are presented in Fig. 6. The absorption peak of pure TiO_2 at 380–780 nm could be found as anatase TiO_2 and the band gap energy (E_g) was 3.1 eV, which displayed visible light absorption and low E_g (3.2 eV) due to the incorporation of N or C with $(NH_4)_2CO_3$.The absorption intensities of Bi_2O_3 with the E_g of approximately 2.9 eV in the visible region from 380 to 450 nm were markedly higher than those in other visible regions. Bi_2O_3 displayed visible light absorption and low E_g, and it exhibited the worse activity than other samples due to the rapid recombination of photogenerated e^- and h^+. Therefore, Bi_2O_3 couldn't be used independently as an oxide catalyst for HCHO oxidation and it needed to be combined with other semiconductors, such as TiO_2, to form heterojunctions structure or others to improve the oxidation activity. In terms of Bi-doped TiO_2 samples, Bi^{3+}/TiO_2 with the E_g of around 3.0 eV exhibited the highest absorption at UV and visible regions, so it showed the highest activity for HCHO degradation at ambient temperature. Bi_2O_3-N/TiO_2 and Bi_2O_3-C/TiO_2 displayed almost the same visible light absorption and E_g (2.8 eV) owing to the rapid recombination of photogenerated e^- and h^+ with Bi_2O_3. Therefore, the samples of Bi_2O_3-N/TiO_2 and Bi_2O_3-C/TiO_2 displayed poor activities for HCHO oxidation. The above results were all consistent with the activity of Bi-doped TiO_2 for HCHO oxidation.

The PL spectra were designed to evaluate the excited state of photocatalysts and the recombination rate of photoinduced e^- and h^+. In this study, the excitation wavelength was 325 nm at room temperature and examined in the range of 350-900 nm with a single scan mode. Fig. 6(C) shows the PL spectra of Bi_2O_3-N/TiO_2, Bi_2O_3-C/TiO_2, Bi^{3+}/TiO_2 and Bi_2O_3-TiO_2. Among these four samples, Bi_2O_3-C/TiO_2 exhibited the highest PL intensity, indicating that Bi_2O_3-C/TiO_2 showed a high recombination rate of photoinduced e^- and h^+, which was not beneficial to increase the activity for photocatalytic oxidation of HCHO. While, compared with Bi_2O_3-N/TiO_2, Bi^{3+}/TiO_2 displayed a lower PL intensity, implying that Bi^{3+}/TiO_2 could improve charge separation with a low recombination rate of e^- and h^+. This was mainly due to the Bi^{3+} doping on TiO_2, which can capture photogenerated e^- from the surface of $Bi_4Ti_3O_{12}$ to reduce charge recombination. This result indicates that Bi^{3+}/TiO_2 can exhibit a higher photocatalytic activity due to that Bi^{3+} doping TiO_2 hinders free carriers from recombination under irradiation. Although Bi_2O_3-TiO_2 showed the lowest PL intensity, the photocatalysts of Bi_2O_3 composite was not conducive to photocatalytic oxidation of HCHO. The above results show that the critical factor to determine the activity of these photocatalysts was Bi^{3+}/TiO_2 that was composed of TiO_2 and $Bi_4Ti_3O_{12}$, confirmed by XRD.

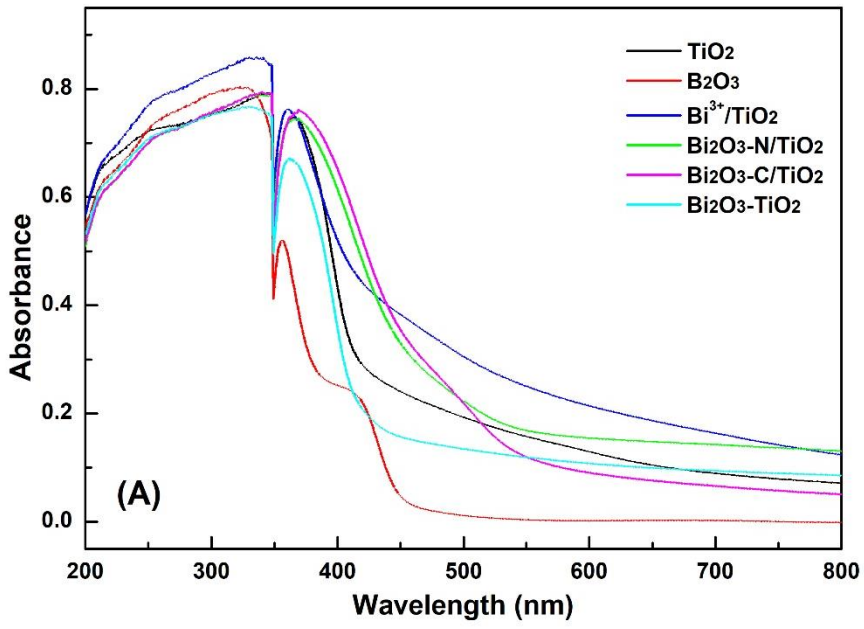

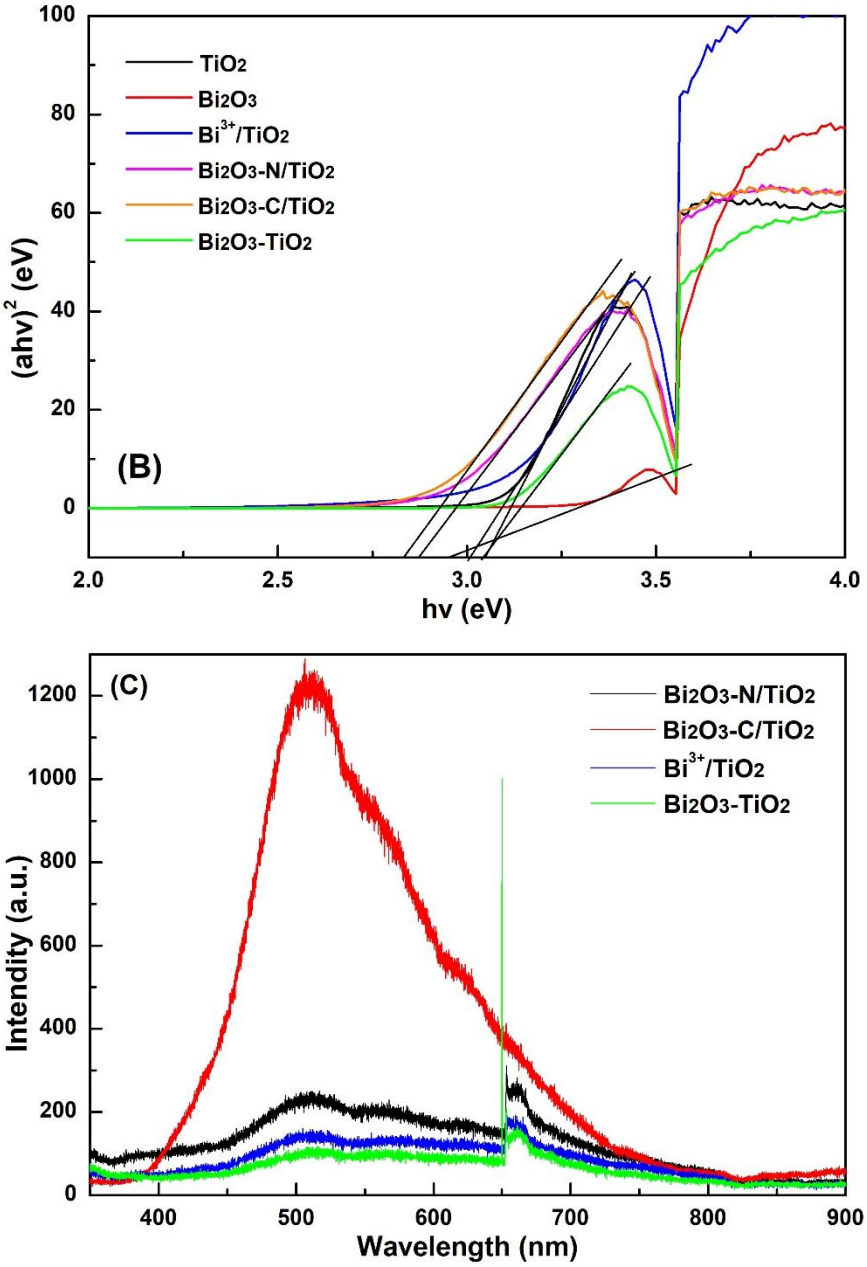

383

384

385 Fig. 6. Diffuse reflectance UV-vis and PL spectra of TiO_2, Bi_2O_3, and Bi-doped TiO_2 catalysts

386 *3.7 XPS analysis*

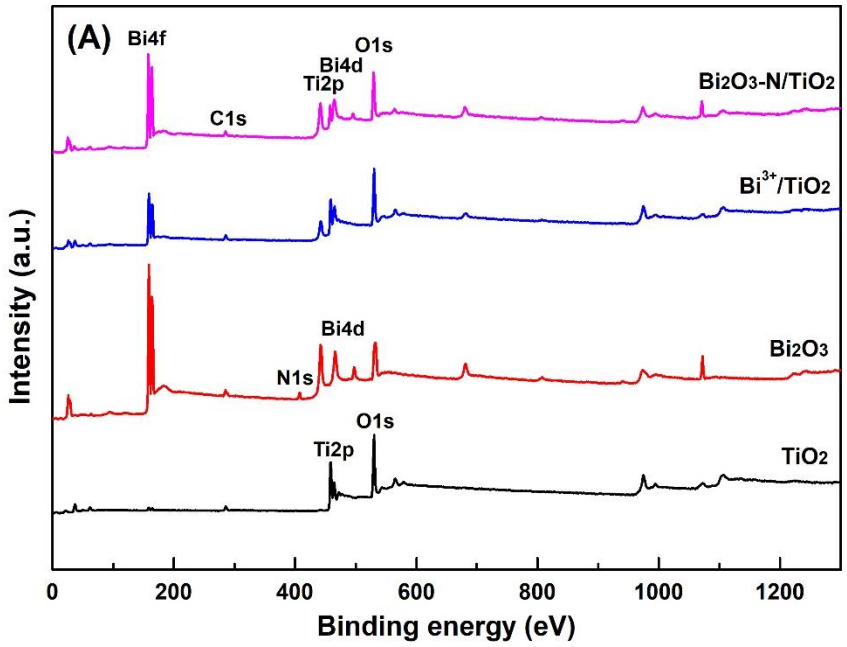
(A)
Bi4f
C1s
Ti2p
Bi4d
O1s
Bi2O3-N/TiO2
Bi3+/TiO2
Bi2O3
N1s
TiO2
Intensity (a.u.)
0
200
400
600
800
1000
1200
Binding energy (eV)

387

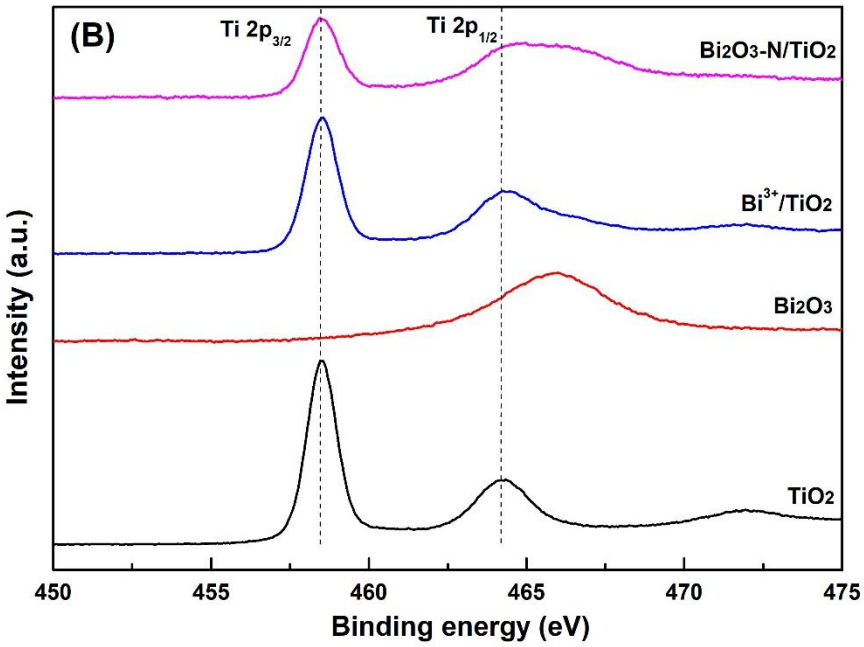
(B)
Ti 2p3/2
Ti 2p1/2
Bi2O3-N/TiO2
Bi3+/TiO2
Bi2O3
TiO2
Intensity (a.u.)
450
455
460
465
470
475
Binding energy (eV)

388

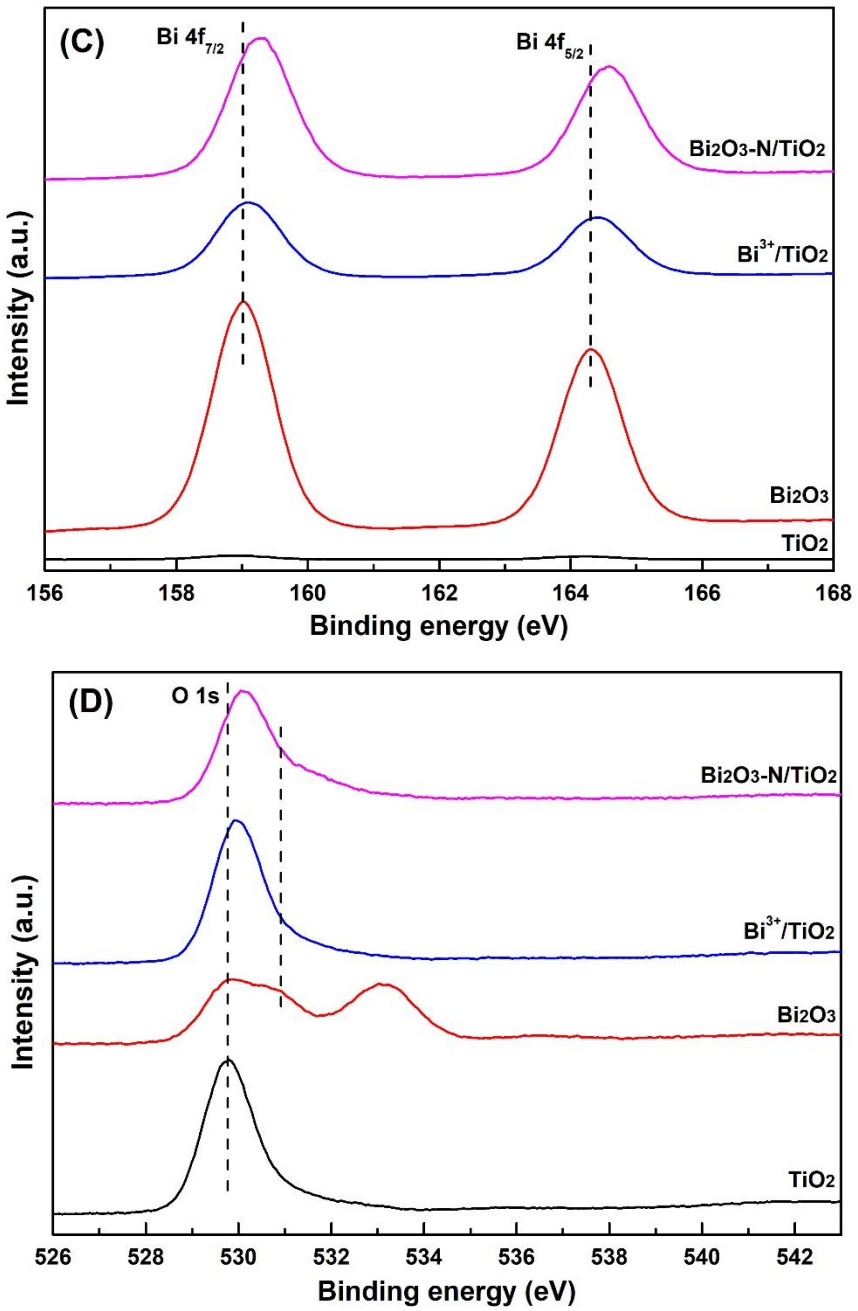

Fig. 7. XPS spectra of different types of TiO_2, Bi_2O_3, and Bi-doped TiO_2 catalysts

The chemical states of TiO_2, Bi_2O_3, and Bi-doped TiO_2 catalysts were detected by using XPS analysis. Ti, Bi, O, C and N elements could be observed on the surface of samples (Fig. 7). The Ti $2p_{3/2}$ and T $2p_{1/2}$ for TiO_2 and Bi^{3+}/TiO_2 were situated at a binding energy (BE) of 458.5 eV and 464.2 eV, respectively. However, the BE of T $2p_{1/2}$ for Bi_2O_3-N/TiO_2 was shifted to high binding energy due to the influence of Bi_2O_3 [39]. The results implied that Bi^{3+}/TiO_2 and Bi_2O_3-N/TiO_2 consisted of TiO_2 and Bi_2O_3, and these were all consistent with XRD analysis. Interestingly, the Bi 4f photoelectron peaks of

Bi-doped TiO_2 had a positive shift to a high BE with pure Bi_2O_3, indicating that the introduction of Bi could induce a strong interplay and e^- transferred between TiO_2 and Bi_2O_3 to generate composite oxides ($Bi_4Ti_3O_{12}$). Among them, Bi_2O_3-N/TiO_2 was the most obvious and Bi^{3+}/TiO_2 was the second, and the result was in agreement with UV-vis and PL spectra. The XPS of the O 1s were also detected. The O 1s levels for TiO_2 and Bi_2O_3 were markedly different and fell to 529.8 eV and 533.1 eV, respectively. In general, the O 1s could be deconvoluted into three contributions [7]: one with the BE of 529.8-529.3 eV indicated to lattice oxygen (O_{lat}), and the other two with BE of 531.6-530.8 and 534.3-532.2 eV assigned to surface adsorbed oxygen (O_{sur}) (O_2^{2-} or O^-) and oxygen species, such as OH. The Bi^{3+}/TiO_2 and Bi_2O_3-N/TiO_2 displayed a higher BE of lattice oxygen, indicating that e^- transfer between TiO_2 and Bi_2O_3. Moreover, the amount of O_{sur} could be increased due to Bi doping. The above measurements indicated the charge transfer between Ti, Bi and O occurring with Bi doping.

3.8 In-situ DRIFTS and IR spectral characteristics

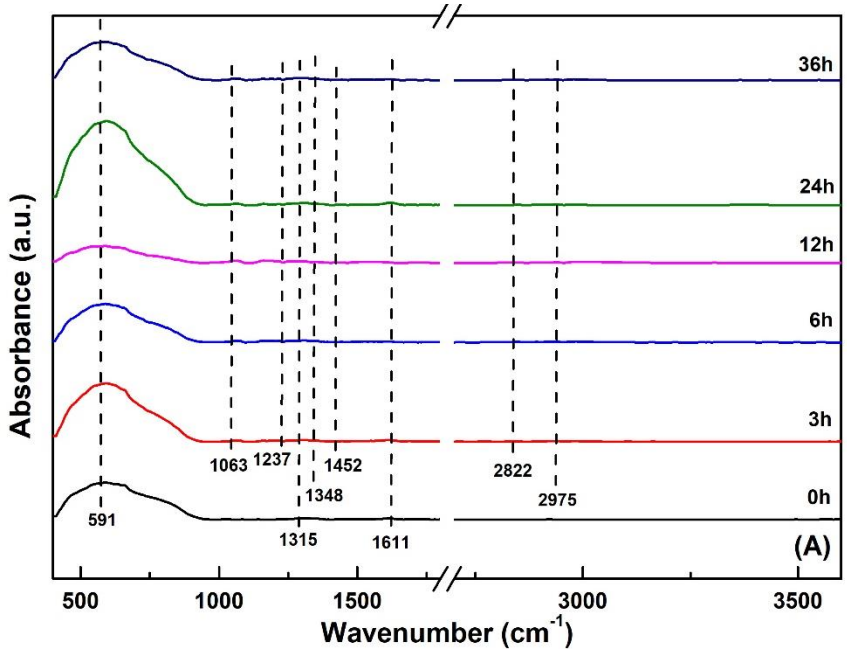

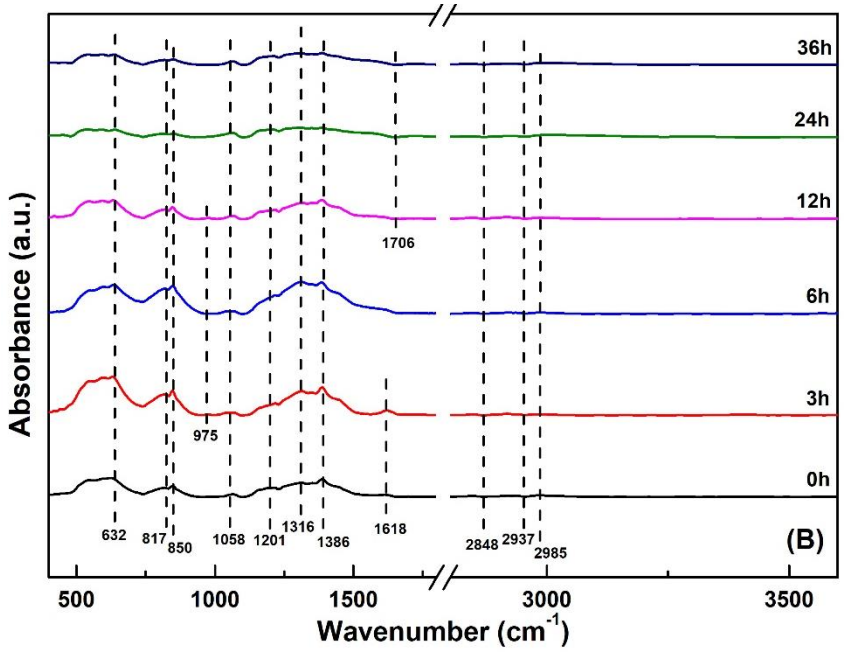
Absorbance (a.u.)
36h
24h
12h
6h
3h
0h
1706
975
632
817
850
1058
1201
1316
1386
1618
2848
2937
2985
(B)
500
1000
1500
3000
3500
Wavenumber (cm-1)

414

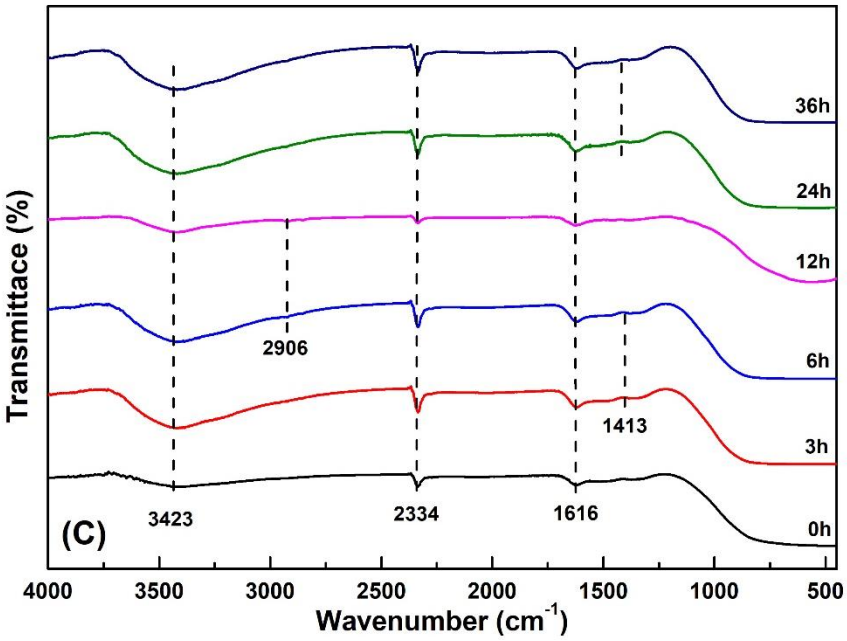
Transmittace (%)
36h
24h
12h
6h
3h
0h
2906
1413
3423
2334
1616
(C)
4000
3500
3000
2500
2000
1500
1000
500
Wavenumber (cm-1)

415

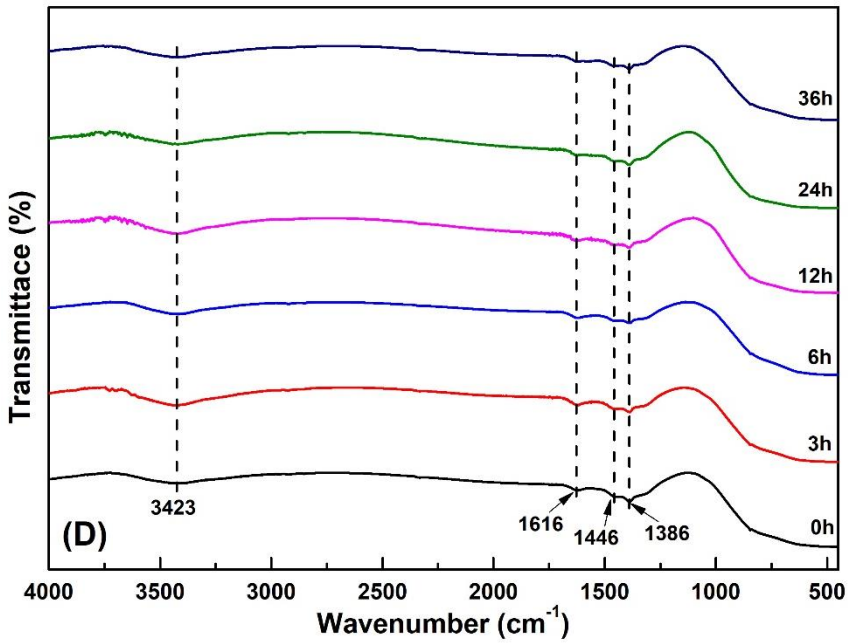

Fig. 8. In-situ DRIFTS and IR spectrum for (A, C) Bi^{3+}/TiO_2, and (B, D) Bi_2O_3-N/TiO_2 catalysts with the different reaction time

Base on the In-situ DRIFTS spectra of Bi^{3+}/TiO_2 and Bi_2O_3-N/TiO_2, as shown in Fig. 8A) and Fig. 8(B), upon exposure to a mixed flow of HCHO/O_2 (1.05 ± 0.05 mg/m^3) with different reaction time (0, 3, 6, 12, 24, and 36h) and different bands, such as 591, 1063, 1160, 1237, 1315 cm^{-1} and others could be observed. According to references [1, 2, 8, 9, 14, 42], as for Bi^{3+}/TiO_2, the bands at 591 and 1315 cm^{-1} of Bi^{3+}/TiO_2 can be assigned to the asymmetric stretching vibration of Ti-O-Ti and stretching vibration of Ti-O, respectively [42]. The bending vibration of water at ca. 1611 cm^{-1} and the characteristic bands of molecularly adsorbed HCHO at 1063 cm^{-1} were found in the Bi^{3+}/TiO_2 [14]. The band at 1348 and weak bands at 2822 and 2975 cm^{-1} were attributed to the symmetric ν_s(COO) and ν_s(CH) stretching of formate [1]. In addition, a broad negative band at ca. 1237 and 1452 cm^{-1} were ascribed to $\nu_s(CH_2)$ and $\delta(CH_2)$ vibration of dioxymethylene (DOM) [2]. The results implied that formate and DOM species were the main intermediates for photocatalytic oxidation of HCHO. As for Bi_2O_3-N/TiO_2 (Fig. 8(B)), the characteristic bands with different reaction time were almost the same as Bi_2O_3-N/TiO_2(0h) without significant changing. The bending vibration of H_2O at 1618 cm^{-1} and the characteristic bands of molecularly adsorbed HCHO at 1058 cm^{-1} were also discovered. Meanwhile, the bands at 1386, 2848 and 2985 cm^{-1} were also ascribed

to the symmetric ν_s(COO) and ν_s(CH) stretching of formate. With the prolonging reaction time, the band at 1618 cm^{-1} corresponding to the bending vibration of OH^- in water adsorbed decreased and the band at 1710 cm^{-1} assigned to the ν(CO) vibration mode of HCHO emerged.

The analysis of water absorption and surface hydroxyl showed the IR spectrum of Bi^{3+}/TiO_2 and Bi_2O_3-N/TiO_2 (Fig. 8(C) and Fig. 8(D)). The results seemed to no significant of water absorption and surface hydroxyl change with the reaction time. The stretching vibration at ca. 3423 cm^{-1} corresponded to the hydroxyl group and the bending vibration at ca. 1616 cm^{-1} was attributed to OH- from the adsorption of H_2O. However, Bi^{3+}/TiO_2 exhibited markedly higher H_2O adsorption than Bi_2O_3-N/TiO_2. In addition, the performance of H_2O adsorption could be increased with reaction time, and thus it displayed a higher activity for HCHO oxidation. Due to the inadequate photocatalytic oxidation of HCHO at 3-36h, two absorption bands at ca. 1413 cm^{-1} and 2906 cm^{-1} suited to the symmetric or other C–H orientations stretching vibration of formate (V_s (COO^-)) were detected. Furthermore, the bands appearing at around 2334 cm^{-1}, 1386 cm^{-1}, and 1446 cm^{-1} can be assigned to the stretching or bending vibration of C-O (V_s (HCO_3^-)) and δ(CH_2) vibration of dioxymethylene (DOM) due to the photocatalytic oxidation reaction. The above results confirmed the presence of surface hydroxyls (OH^-) in the structure of these two samples and revealed that the importance of surface hydroxyls on HCHO degradation, especially for Bi^{3+}/TiO_2. These adsorbed H_2O and OH^- are crucial to improve the activity for HCHO oxidation due to their reaction with the photogenerated hole on the surface and the formation of hydroxyl radicals. As the above data of In-situ DRIFTS and IR and reported in literatures [1, 2, 8, 9, 14, 42, 43, 44], HCHO was degraded into dioxymethylene (DOM) at first, and then further into formate and carbonate, then finally desorbs as CO_2.

3.9 EPR spectroscopy

To understand the roles of reactive oxygen species such as $^{\bullet}O_2^-$ and •OH in the photocatalytic process, EPR technique was used to detect the characteristics and active radicals in the samples. As shown in Fig. 9, the value of g=2.003 was ascribed to the paramagnetic characteristic value of $^{\bullet}O_2^-$ [45], and the value of paramagnetic

characteristic could be increased by Bi^{3+} doping with TiO_2. Bi^{3+}/TiO_2 displayed the highest amount of $^{\bullet}O_2^-$, followed by TiO_2, Bi_2O_3-N/TiO_2, and Bi_2O_3. The results showed that the types and amount of Bi doping played an important role in the change of $^{\bullet}O_2^-$ concentration. When Bi_2O_3 doped in TiO_2, some of Bi_2O_3 exposed as an electrically charged composite centre, which prevented some e^- from being trapped by oxygen vacancies. The reduce of charged oxygen vacancies resulted in the reduction of the amount of $^{\bullet}O_2^-$ [29]. Therefore, when the amount of $^{\bullet}O_2^-$ decreased, the peak strength on the paramagnetic characteristic of $^{\bullet}O_2^-$ and the activity decreased, which was consistent with the results of photocatalytic oxidation of HCHO.

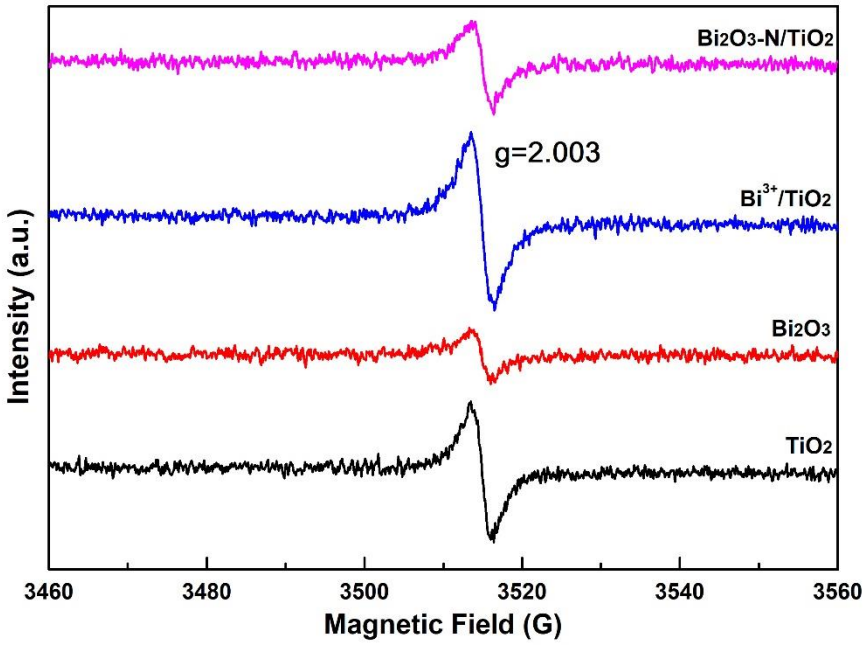

Fig. 9. EPR spectra of different types of TiO_2, Bi_2O_3, and Bi-doped TiO_2 catalysts

3.10 Mechanisms for photocatalytic oxidation of HCHO

Depending on the structure of Bi-doped TiO_2, particularly for Bi^{3+}/TiO_2, the structure of heterojunction, identified as $Bi_4Ti_3O_4$ and TiO_2, could promote efficient charge separation, with the consequence of reducing the recombination of photogenerated e^- and h^+ (Fig. 10). Gan et al. found UV-vis DRS, the E_{bg} for $Bi_4Ti_3O_4$ and TiO_2 were about 2.91 eV and 3.1 eV [46]. Therefore, the E_{cb} and E_{vb} for $Bi_4Ti_3O_4$ and TiO_2 were calculated as -0.41 eV, -0.12 eV, 2.50 eV and 2.98 eV, respectively. Because the E_{cb} of TiO_2 was lower than $Bi_4Ti_3O_4$, the photogenerated e^- could be moved easily from $Bi_4Ti_3O_4$ to TiO_2. The holes transferred in the opposite direction and thus depressed the

recombination of e^- and h^+. Moreover, the formation of formate species (2822 and 2975 cm^{-1}) and dioxymethylene (1237 and 1452 cm^{-1}), ascribed to the results of in-situ DRIFTS spectra, could be found clearly in the Bi^{3+}/TiO_2. These two kinds of species, identified as by-products of photocatalytic oxidation, could also be observed by IR spectrum. On the other hand, the weak band at 1710 cm^{-1} corresponding to the ν(CO) vibration of HCHO could be observed on the surface of catalysts. More importantly, the intensity of stretching vibration at ca. 3423 cm^{-1} assigned to the hydroxyl group decreased with the extension of reaction time.

According to the above investigations, the adsorption of HCHO on the surface was the first step in the catalytic reaction. Bi^{3+}/TiO_2 was activated by the visible light and the photogenerated e^- and h^+ could be transferred by the heterojunction structure. Then, these e^- can react with O_2 to generate superoxide radical anion ($^{\bullet}O_2^-$), which can oxidize HCHO into the DOM and formate species. The formate can further break up into CO and H_2O, and CO could be further oxidized to CO_2 [2, 47]. Another possible pathway is that these photogenerated holes can be combined with OH^- or H_2O to generate hydroxyl radical (•OH), which could directly oxidize HCHO or formate into CO_2 and H_2O and tackle the environmental pollution [48, 49].

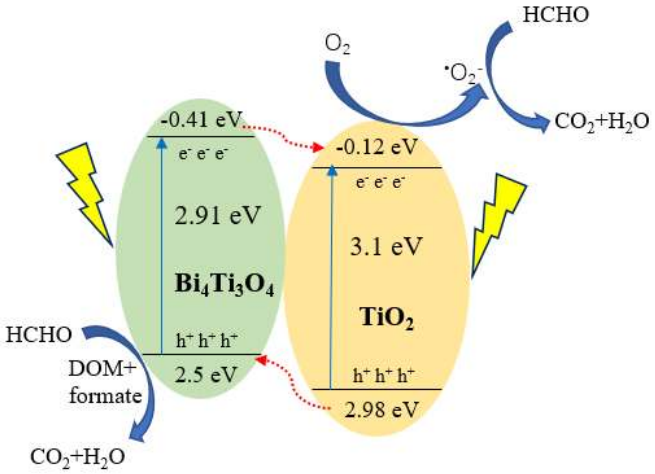

Fig. 10. Proposed electron–hole pair separation in the Bi^{3+}/TiO_2 composites under visible irradiation

4. Conclusions

In this study, a serious of Bi-doped TiO_2 catalysts were synthesized by sol using the hydrothermal method, and then promoted for the photocatalytic degradation of HCHO

under visible light irradiation and ambient temperature. Compared with pure TiO_2 and Bi_2O_3, photocatalytic oxidation of HCHO can be further improved by the Bi-doped TiO_2 catalysts, especially Bi^{3+}/TiO_2. According to the investigation of characterization, it could be observed that the excess Bi_2O_3 doping into TiO_2 catalysts, such as Bi_2O_3-N/TiO_2 and Bi_2O_3-C/TiO_2, formed a mixed oxides with Bi_2O_3 and $Bi_4Ti_3O_{12}$, and they were disadvantage to enhance the activity. However, Bi^{3+}/TiO_2 composed of TiO_2 and $Bi_4Ti_3O_{12}$ displayed a higher activity and remained good stability for HCHO oxidation. It was worth mention that Bi^{3+}/TiO_2 didn't have the lowest binding energy, but it displayed a lower PL intensity. The highest activity mainly depends on the uniform particulates, high surface areas, and the great interaction between TiO_2 and $Bi_4Ti_3O_{12}$ via charge transfer.

In summary, this study demonstrated that HCHO can be effectively oxidized to 0.058 mg/m^3 (94.7%) at visible light excitation within 36 h. The heterogeneous catalysts with TiO_2 and $Bi_4Ti_3O_{12}$ were the main critical factor to degrade gaseous organic pollutants. The results made new contribution for a better understanding of the existing state of Bi in the TiO_2 crystal.

Acknowledgements

This work was financially supported by the Natural Science Foundation of Jiangsu Province (Nos. BK20170954 and BK20150890), the National Natural Science Foundation of China (Nos. 21501097), the Qing Lan Project of the Jiangsu Higher Education Institutions of China, the Priority Academic Program Development of Jiangsu Higher Education Institutions (PAPD), the Top-notch Academic Programs Project of Jiangsu Higher Education Institutions (PPZY2015C222), the Jiangsu Engineering Technology Research Centre of Environmental Cleaning Materials and Open Research Fund Program of Jiangsu Key Laboratory of Atmospheric Environment Monitoring & Pollution Control (KHK1806), A projected funded by the Priority Academic Program Development of Jiangsu Higher Education Institutions (PAPD).

References

[1] F. Liu, S.P. Rong, P.Y. Zhang, L.L. Gao. Appl. Catal. B 235 (2018) 158.

[2] D. Sun, S. Wageh, A.A. Al-Ghamdi, Y. Le, J.G. Yu, C.J. Jiang. Appl. Surf. Sci. 466 (2019) 301.

[3]V. Binas, V. Stefanopoulos, G. Kiriakidis, P. Papagiannakopoulos. J. Mater. 5 (2019) 56.

[4] A. Okawa, R. Yoshida, T. Isozaki, Y. Shigesato, Y. Matsushita, T. Suzuki. Catal. Commun. 100 (2017) 1.

[5] X.A. Dong, W. Cui, H. Wang, J.Y. Li, Y.J. Sun, H.Q. Wang, Y.X. Zhang, H.W. Huang, F. Dong. Sci. Bull. 64 (2019) 669.

[6] J.Y. Li, X.A. Dong, G. Zhang, W. Cui, W.L. Cen, Z.B. Wu, S. C. Lee, F. Dong. J. Mater. Chem. A 7 (2019) 3366.

[7] Z. Zhang, J. Huang, H.Q. Xia, Q.G. Dai, Y.F. Gu, Y.J. Lao, X.Y. Wang. J. Catal. 360 (2018) 277.

[8] Z.X. Yan, Z.H. Xu, Z.H. Yang, L. Yue, L.Y. Huang. Appl. Surf. Sci. 467 (2019) 277.

[9] Y. Zhang, M.X. Chen, Z.X. Zhang, Z. Jiang, W.F. Shangguan, H. Einaga. Catal. Today. 327 (2019) 323.

[10] D. Kibanova, M. Sleiman, J. Cervini-Silva, H. Destaillats. J. Hazard. Mater. 211 (2012) 233.

[11] X.Q. Deng, J.L. Liu, X.S. Li, B. Zhu, X.B. Zhu, A.M. Zhu. Catal. Today. 281 (2017) 630.

[12] J.Y. Li, W. Cui, P. Chen, X.A. Dong, Y.H. Chu, J.P. Sheng, Y.X. Zhang, Z.M. Wang, F. Dong. Appl. Catal. B 260 (2020) 118130.

[13] X.S. Li, X.Y. Ma, J.L. Liu, Z.G. Sun, B. Zhu, A.M. Zhu. Catal. Today. 337 (2019) 132.

[14] S.Y. Huang, B. Cheng, J.G. Yu, C.J. Jiang. ACS Sustain. Chem. Eng. 6 (2018) 12481.

[15] G.K. Zhang, Q. Xiong, W. Xu, S. Guo. Appl. Clay. Sci. 102 (2014) 231.

[16] M. Malayeri, F. Haghighat, C.S. Lee. Build. Environ. 154 (2019) 309.

[17] G.X. Zhang, Z.M. Sun, Y.W. Duan, R.X. Ma, S.L. Zheng. Appl. Surf. Sci. 412 (2017) 105.

[18] X. Li, X.R. Qian, X.H. An, J.W. Huang. Appl. Surf. Sci. 487 (2019) 1262.

[19] R.F. Liu, W.B. Li, A.Y. Peng. Appl. Surf. Sci. 427 (2018) 608.

[20] M. He, J. Ji, B.Y. Liu, H.B. Huang. Appl. Surf. Sci. 473 (2019) 934.

[21] T. Ohno, M. Akiyoshi, T. Umebayashi,K. Asai, T. Mitsui, M. Matsumura. Appl. Catal. A 265 (2004) 115.

[22] X.Y. Pan, Y.J Xu. J. Phys. Chem. C. 117 (2013) 17996.

[23] J. Li, M. Zhang, Q.Y. Li, J.J. Yang. Appl. Surf. Sci. 391 (2017) 184.

[24] C. Huang, Y. Ding, Y.W. Chen, P. Li, S.B. Shen. J. Environ. Sci. 60 (2017) 61.

[25] S.H. Liu, W.X. Lin. J. Photoch. Photobio. A 378 (2019) 66.

[26] W. Low, V. Boonamnuayvitaya. J. Environ. Manage. 127 (2013) 142.

[27] J.P. Li, D.J. Ren, Z.X. Wu, J. Xu, Y.J. Bao, S. He, Y.H. Chen. J. Colloid. Inter. Sci. 530 (2018) 78.

[28] Q. Huang, P. Wang, Y.Z. Fan, Q. Wang. Indoor. Built. Enviro. 26 (2017) 785.
[29] Y.F. Huang, Y.L. Wei, J. Wang, D. Luo, L.Q. Fan, J.H. Wu. Appl. Surf. Sci. 423 (2017) 119.
[30] Y.B. Liu, G.Q. Zhu, J.Z. Gao, M. Hojamberdiev, R.L. Zhu, X.M. Wei, Q.M. Guo, P. Liu. Appl. Catal. B 200 (2017) 72.
[31] S. Murcia-López, M. Hidalgo, J.A. Navío. Appl. Catal. A 404 (2011) 59.
[32] B. Benalioua, M. Mansour, A. Bentouami, B. Boury, E.H. Elandaloussi. J. Hazard. Mater. 288 (2015) 158.
[33] A. Hamdi, A.M. Ferraria, A.M. Botelho Rego, D.P. Conceicao, L.F. Vieira Ferreira, S. Bouattour. J. Mol. Catal. A 380 (2013) 34.
[34] L.W. Lu, M.L Lv, D. Wang, G.Liu, X.X. Xu. Appl. Catal. B 200 (2017) 412.
[35] J.H. Lee, H. Lee, M.J. Kang. Mater. Lett. 178 (2016) 316.
[36] J. Zhu, S.H. Wang, J.G. Wang, D.Q. Zhang. Appl. Catal. B 102 (2011) 120.
[37] C.C. Pei, W.W.F. Leung. Appl. Catal. B 174 (2015) 515.
[38] J.Z. Wang, H.L. Li, X.R. Yan, C. Qian, Y.J. Xing, S.T. Yang, Z.K. Kang, J.Y. Han, W.X. Gu, H.Y. Yang, F.J. Xiao. J. Alloys. Compounds. 795 (2019) 120.
[39] Y. Hu, Y.T. Cao, P.X. Wang, D.Z. Li, W. Chen, Y.H. He, X.Z. Fu, Y. Shao, Y. Zhang. Appl. Catal. B 125 (2012) 294.
[40] T.V.L. Thejaswini, D. Prabhakaran, M.A. Maheswari. J. Environ. Chem. Eng. 4 (2016) 1308.
[41] Q. Huang, Q. Wang, T. Tao, Y.X. Zhao, P. Wang, Z.Y. Ding, M.D. Chen. Environ. Technol. 40 (2019) 1937.
[42] H.S. Zuo, J. Sun, K.J. Deng, R. Su. Chem. Eng. Technol. 30 (2007) 577.
[43]P. Liu, G.L. Wei, H.P. He, X.L. Liang, H.L. Chen, Y.F. Xi, J.X. Zhu. Appl. Surf. Sci. 464 (2019) 287.
[44] P. Liu, G.L. Wei, X.L. Liang, D. Chen, H.P. He, T.H. Chen, Y.F. Xi, H.L. Chen, D.H. Han, J.X. Zhu. Appl. Clay. Sci. 161 (2018) 265.
[45] C.P. Kumar, N.O. Gopal, T.C. Wang, M.S. Wong, S.C. Ke. J. Phy. Chem. B 110 (2006) 5223.
[46] H.H. Gan, F.T. Yi, H.N. Zhang, Y.X. Qian, H.X. Jin, K.F. Zhang. Chinese. J. Chem. Eng. 26 (2018) 2628.
[47] Y. Ma, G.K. Zhang. Chem. Eng. J. 288 (2016) 70.
[48]. H. Yang, X. Huang, J.R. Thompson, R.J. Flower. Science 347 (2015) 834.
[49]. H. Yang. Nature 509 (2014) 535.